Research Square

Preprints are preliminary reports that have not undergone peer review.
They should not be considered conclusive, used to inform clinical practice,
or referenced by the media as validated information.

Concentration-Dependent Solvation Structure, Ion Association and Transport in Aqueous $ZnCl_2$ Electrolytes: A Self-Consistent Force- Field Study with Effective Charge Scaling

Dan Ji

pachydan@outlook.com

Neijiang Normal University

Xiaolin Li

Neijiang Normal University

Yue Yu

Neijiang Normal University

Research Article

Keywords: zinc chloride, aqueous electrolyte, molecular dynamics, ion pairing, solvation shell

Posted Date: November 12th, 2026

DOI: https://doi.org/10.21203/rs.3.rs-11472069/v1

License: This work is licensed under a Creative Commons Attribution 4.0 International License.
Read Full License

Additional Declarations: No competing interests reported.

Concentration-Dependent Solvation Structure, Ion Association and Transport in Aqueous $ZnCl_2$ Electrolytes: A Self-Consistent Force-Field Study with Effective Charge Scaling

Dan Ji*, Xiaolin Li, Yue Yu

College of Chemistry and Environmental Engineering, Neijiang Normal University, Neijiang, 641100, PR China

Corresponding author: Dan Ji, e-mail: pachydan@outlook.com

Abstract Concentrated aqueous $ZnCl_2$ solutions determine the stability of mild zinc batteries, yet how rising salt concentration reshapes the Zn^{2+} first solvation shell and ion association, and whether a classical non-polarizable force field can describe this behaviour, remain controversial. Here we ran all-atom molecular dynamics simulations of aqueous $ZnCl_2$ at four concentrations (1–10 mol·kg^{-1}) at 298.15 K and 1 bar, with three independent replicas and sampling long enough to permit ligand exchange at every concentration. The simulations reproduce the experimental first-shell structure: with rising concentration, water is progressively displaced from the first coordination sphere by chloride, and the speciation evolves from the octahedral hexa-aqua complex $[Zn(H_2O)_6]^{2+}$ toward higher chloro-complexes such as $[ZnCl_3]^-$ and $[ZnCl_4]^{2-}$. Self-diffusion of all species decreases with concentration, while the Nernst–Einstein conductivity first rises and then declines, reproducing the experimentally reported maximum near 6 mol·kg^{-1}. Finally, an effective-charge-scaling (ECC) boundary test shows that charge scaling alone erases Zn–Cl contact ion pairing, and only its combination with a dedicated Zn–Cl term retains physically meaningful association. These results quantify the minimum physics a classical model requires for a quantitative description of concentrated $ZnCl_2$ electrolytes.

Keywords zinc chloride · aqueous electrolyte · molecular dynamics · ion pairing · solvation shell

1 Introduction

Aqueous zinc batteries are a leading chemistry for safe, low-cost and scalable electrochemical energy storage, owing to intrinsic safety of the aqueous electrolyte, high theoretical capacity of the zinc metal anode, and relative abundance of zinc [1, 2, 3]. Aqueous zinc-ion batteries employ mildly concentrated Zn salt solutions as electrolytes; $ZnCl_2$ is attractive for its high solubility, low cost and environmental benignity [4, 5]. In dilute solution Zn^{2+} is fully hydrated as the octahedral $[Zn(H_2O)_6]^{2+}$ complex [6, 7]. As salt loading rises, the limited number of water molecules per ion can no longer maintain the full hydration shell, so chloride enters the first coordination sphere (dehydration-chloride substitution), the free-water activity decreases, and ion pairs and larger associates form [8, 9]. These structural changes suppress water decomposition, alter the hydrogen-bond network, and control ionic mobility and the resulting conductivity [10, 11].

Molecular dynamics is a primary tool for resolving this concentration-dependent solvation [12, 13, 14]. Two issues dominate recent debate: (1) many classical reports pair a general-purpose force field with a mismatched water model and unscaled full ionic charges, yielding Zn–Cl association that is not quantitatively reliable [15, 16, 17]; and (2) the partly covalent, short (~0.225 nm) Zn–Cl bond is genuinely difficult for non-polarizable force fields, which tend either to over-bind the contact pair (full charges, no polarization) or to erase it entirely when the charges are scaled without a compensating specific term [18]. Duboué-Dijon et al. [18] showed with neutron scattering and ab initio molecular dynamics that a scaled-charge (ECC) Zn^{2+} parameter set plus a dedicated Zn–Cl Lennard-Jones term reproduces the experimental solution structure, while neither full-charge

nor charge-only ECC does. Machine-learned potentials have recently been pushed into these concentrated regimes, confirming the same structural picture while remaining computationally demanding [19, 20, 21, 22].

Here we adopt this validated self-consistent force field (SPC/E water + ECC Zn/Cl + specific Zn–Cl term) and run a uniform 1–10 mol·kg^{-1} $ZnCl_2$ series with independent replicas long enough (20 ns at 1–3 mol·kg^{-1}; 50 ns at 6–10 mol·kg^{-1}) that ligand exchange is accessible at every concentration in order to resolve two weaknesses common to such studies: force fields that are not internally self-consistent, and simulations too short for ligand-exchange equilibration at the highest concentrations. We then (i) map the monotonic dehydration–chloride substitution and coordination-number evolution across the full series; (ii) quantify the first-shell species $[Zn(H_2O)_xCl_\gamma]^z$ at all four concentrations; (iii) estimate self-diffusion and Nernst–Einstein conductivity and test the measured rise-then-fall profile; and (iv) run an ECC charge-scaling boundary test at 1 mol·kg^{-1} to isolate the role of the specific Zn–Cl term. The central methodological message is that effective charge scaling repairs hydration electrostatics but must be combined with a dedicated Zn–Cl interaction to retain ion association, a result that quantifies the minimum physics a classical model needs for aqueous $ZnCl_2$. Sect. 2 describes the self-consistent models and computational methods, Sect. 3 presents and discusses the results, and a brief conclusion is offered in Sect. 5. The concentration range studied here spans the salt-in-water regime relevant to mildly concentrated $ZnCl_2$ electrolytes; the extreme water-in-salt limit ($\gtrsim$ 20 mol·kg^{-1}) is beyond the present scope.

2 Models and Methods

2.1 Force field (self-consistent set)

All simulations used GROMACS 2026.4 [23, 24]. We adopt the self-consistent $ZnCl_2$ parameter set of Duboué-Dijon et al. [18], which was validated against neutron-diffraction-isotopic-substitution (NDIS) data and Born–Oppenheimer ab initio molecular dynamics:

- Water: SPC/E [25], O ε = 0.6502 kJ·mol^{-1}, σ = 0.3166 nm, q(O) = −0.8476, q(H) = +0.4238.

- Ions (ECC, scaled charge) [26, 27]: Zn^{2+} q = +1.5, σ = 0.175 nm, ε = 1.046 kJ·mol^{-1}; Cl^- q = −0.75, σ = 0.410 nm, ε = 0.4928 kJ·mol^{-1}.

- Specific Zn–Cl term: a dedicated Lennard-Jones interaction σ_ZnCl = 0.26 nm, fitted in [18] to the ab initio Zn–Cl free-energy profile (which the standard Lorentz–Berthelot mixing of the ECC self-parameters cannot reproduce). Here its ε is taken as the Lorentz–Berthelot geometric mean of the Zn and Cl self-ε, $\sqrt{(1.046 \times 0.4928)} \approx 0.718$ kJ·mol^{-1} (we note the ε of this specific term is not tabulated in the main text of [18]; see Online Resource 1).

- Other cross-parameters derived by Lorentz–Berthelot mixing.

This removes the earlier non-self-consistent choice (a biomolecular force field [28] paired with SPC water and unscaled full charges) and places the whole concentration series on one internally consistent, experiment-anchored parameter set.

2.2 Systems and protocol

Four boxes were built at target molality 1, 3, 6 and 10 mol·kg^{-1} (Table 1). Energy minimization (steepest descent) → NVT 50 ps (V-rescale [29], 298.15 K) → NPT 400 ps (Parrinello–Rahman [30], 1 bar, compressibility 4.5 × 10^{-5} bar^{-1}) → production. Production ran 20 ns at 1–3 mol·kg^{-1} and 50 ns at 6–10 mol·kg^{-1} per replica (dt = 2 fs, H-bonds constrained, PME electrostatics [31], dispersion correction, Verlet cutoff 0.8 nm). Three independent replicas (gen_seed 101/202/303) were each equilibrated independently, so the error bars reflect independent velocities, equilibration and sampling. The longer high-concentration runs ensure ligand exchange (at 10

mol·kg^{-1}, D(Zn^{2+}) ≈ 0.12 × 10^{-9} $m^2 \cdot s^{-1}$ gives a root-mean-square displacement √(6Dt) ≈ 5.9 nm in 50 ns) and therefore make the speciation analysis statistically meaningful at every concentration.

Table 1 System composition and production length

Box / target molality	N(Zn^{2+})	N(Cl^-)	N(H_2O)	Production
1 mol·kg^{-1}	12	24	666	20 ns × 3
3 mol·kg^{-1}	12	24	222	20 ns × 3
6 mol·kg^{-1}	24	48	222	50 ns × 3
10 mol·kg^{-1}	24	48	133	50 ns × 3

2.3 Analysis

- RDF g(r) and running coordination numbers: Zn–O integration cutoff 0.32 nm, Zn–Cl 0.35 nm (first minima).

- First-shell species [$Zn(H_2O)_xCl_y$] from per-frame nearest-neighbor counting of Cl^- within 0.35 nm (mdtraj); contact ion pair (CIP) = Zn with at least one Cl^- within 0.35 nm.

- Self-diffusion D from the linear (diffusive) region of the ensemble-averaged mean-square displacement (Einstein relation) [32, 33], computed from unwrapped coordinates.

- Nernst–Einstein conductivity $\sigma_NE = (e^2 / k_B\ T\ V)\ \Sigma_i\ N_i\ z_i^2\ D_i$; reported in absolute units ($S \cdot m^{-1}$, Table 4) but interpreted as a relative, concentration-dependent indicator only, because the Nernst–Einstein relation neglects correlated (Onsager) motion; no comparison with experimental absolute conductivities is attempted.

- All values are reported as mean ± standard error over three replicas, except the ECC λ scan (Sect. 2.4), which uses single runs.

2.4 ECC boundary test at 1 mol·kg^{-1}

To isolate the role of the specific Zn–Cl term, on the well-relaxed 1 mol·kg^{-1} box we rescale ionic charges by λ (Zn^{2+} = +2λ, Cl^- = −λ; neutrality preserved) and run short 5 ns simulations at λ = 1.00, 0.95, 0.90, 0.85 and 0.75, in two versions: (a) a charge-only model (Lennard-Jones parameters and the SPC/E water unchanged -the naive ECC used in many studies), and (b) the self-consistent model (scaled charge with the specific Zn–Cl term retained). Comparing the CIP response of the two versions across λ isolates exactly what the specific term contributes.

3 Results and Discussion

3.1 Radial distribution and coordination

The Zn–O RDF first peak sits at 0.209–0.212 nm and stays nearly fixed with concentration while its height declines; the Zn–Cl contact peak at 0.212–0.223 nm grows strongly (Fig. 1). The integrated coordination numbers (Table 2, Fig. 2) show monotonic Zn–O dehydration (5.47 → 2.63) and Zn–Cl uptake (0.50 → 2.20) across the full series. The Zn–O distance matches the experimental/ab initio benchmark (≈ 0.210 nm) [34, 35], consistent with earlier simulations of divalent-ion hydration [36], and the Zn–Cl contact reproduces the short, partly covalent distance (~0.225 nm) that the earlier non-self-consistent model placed too long.

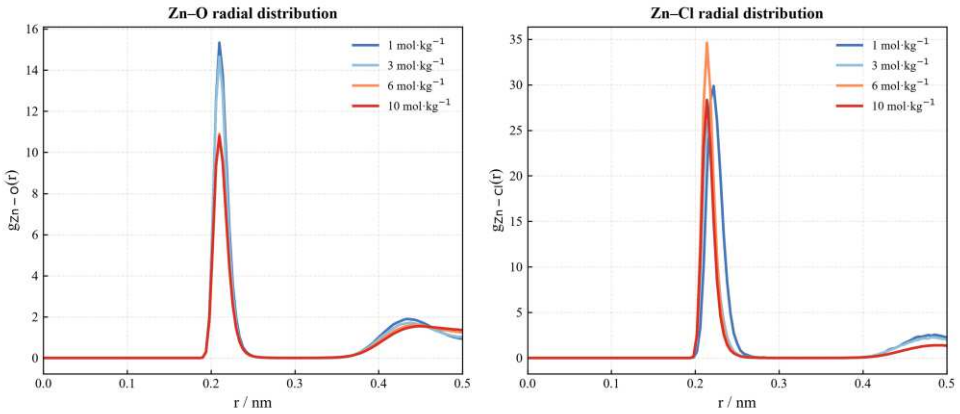


Fig. 1 Radial distribution functions g(r) for Zn–O(water) (left) and Zn–Cl^- (right), averaged over three replicas

Table 2 RDF first-peak position r_max and coordination numbers (mean ± standard error)

molality	r_max (Zn–O) / nm	r_max (Zn–Cl) / nm	CN(Zn–O)	CN(Zn–Cl)
1 mol·kg^{-1}	0.212 ± 0.000	0.223 ± 0.000	5.47 ± 0.02	0.50 ± 0.03
3 mol·kg^{-1}	0.212 ± 0.000	0.214 ± 0.003	4.67 ± 0.52	0.94 ± 0.34
6 mol·kg^{-1}	0.211 ± 0.003	0.212 ± 0.000	3.09 ± 0.05	1.93 ± 0.01
10 mol·kg^{-1}	0.209 ± 0.003	0.212 ± 0.000	2.63 ± 0.03	2.20 ± 0.02

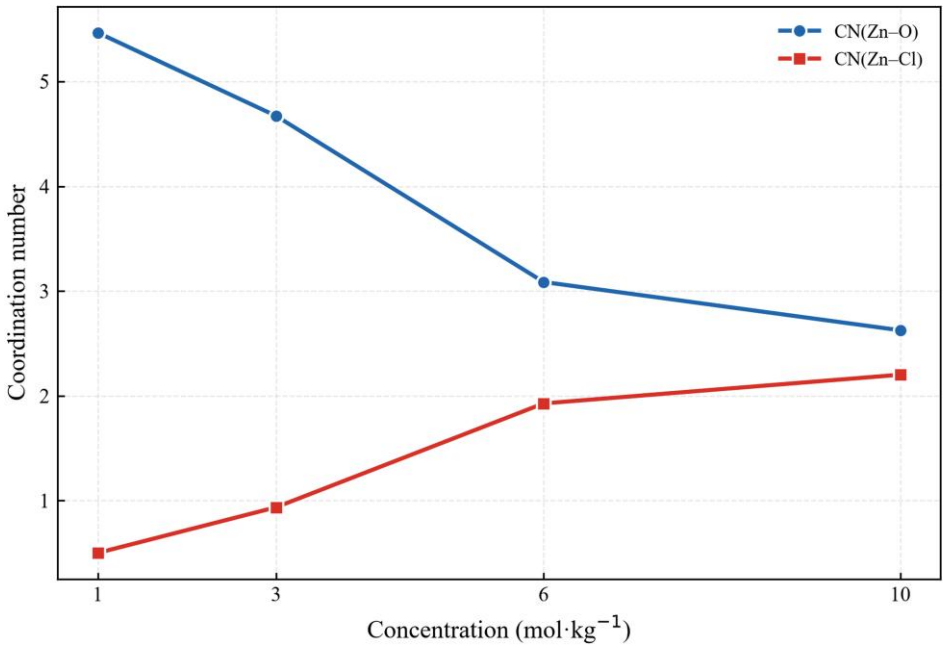


Fig. 2 Coordination numbers CN(Zn–O) and CN(Zn–Cl) versus molality with error bars

3.2 First-shell speciation at all concentrations

Because 50 ns allows ligand exchange even at 10 mol·kg^{-1}, concentration-resolved first-shell species populations are reported at all four concentrations (Fig. 3, Table 3). At 1 mol·kg^{-1} the shell is predominantly $[Zn(H_2O)_6]$-type with a substantial $[ZnCl(H_2O)_5]^+$ population (≈ 46%); with increasing concentration chloride progressively displaces water: at 6 mol·kg^{-1} $[ZnCl_3]^-$ and $[ZnCl_4]^{2-}$ become significant, and at 10 mol·kg^{-1} $[ZnCl_3]^-$ is the dominant species (42.3%) with the $[ZnCl_4]^{2-}$ fraction (12.9%, essentially unchanged from the 13.3% at 6

mol·kg⁻¹). This dehydration–chloride-substitution progression $[Zn(H_2O)_6]^{2+} \rightarrow [ZnCl_3]^-/[ZnCl_4]^{2-}$ matches the species picture reported for aqueous $ZnCl_2$ [15, 16, 37, 38, 39, 40].

Table 3 First-shell species population (%) by molality (mean over replicas)

Species	1 mol·kg^{-1}	3 mol·kg^{-1}	6 mol·kg^{-1}	10 mol·kg^{-1}
$Zn(H_2O)_n$ (no Cl)	52.5	48.9	18.4	8.7
$[ZnCl]^+$	46.0	30.3	31.2	31.2
$[ZnCl_2]$	0.7	2.9	4.4	5.0
$[ZnCl_3]^-$	0.8	13.9	32.7	42.3
$[ZnCl_4]^{2-}$	0	4.0	13.3	12.9

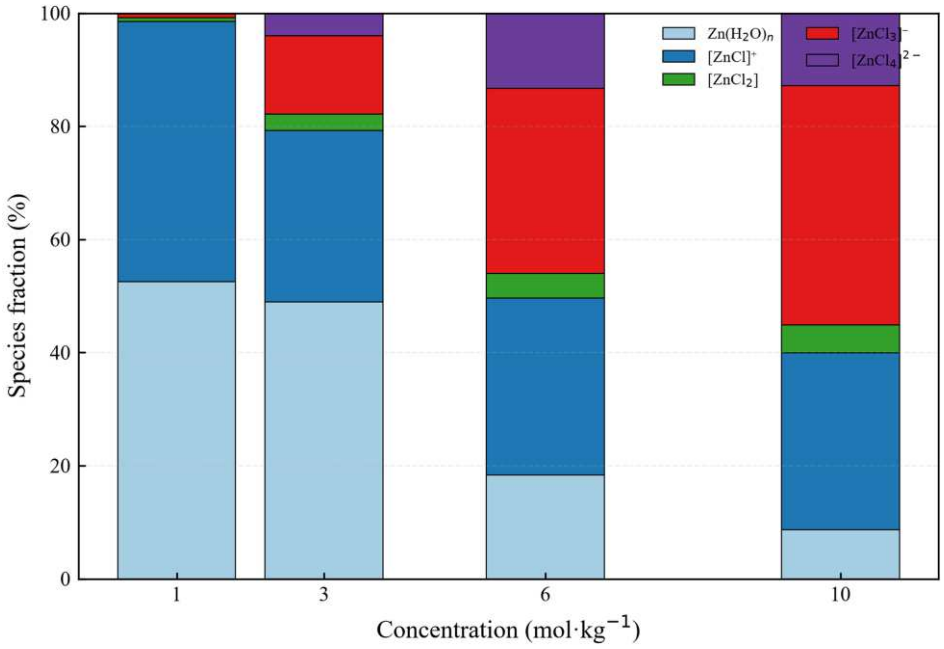


Fig. 3 Stacked species fraction versus molality

3.3 Contact ion pairing

The contact-ion-pair fraction (Zn with at least one Cl^- within 0.35 nm) rises from ≈ 50% at 1 mol·kg^{-1} to a high, plateau-like level at 6–10 mol·kg^{-1}, consistent with the shift toward higher chloro-complexes in Sect. 3.2 [38, 41]. We keep two distinct quantities separate: CIP counts any Cl within the cutoff of a Zn (an electrostatic contact), whereas chloride-bridged multi-Zn aggregates require one Cl to bridge two Zn through a directional bond and remain a minority that we do not over-state (see Sect. 4). Even with the specific Zn–Cl term, the classical model may over-count contact pairs relative to experiment because the partly covalent Zn–Cl bond is represented only by a strengthened Lennard-Jones term [18, 42].

3.4 Diffusion, conductivity and transport

Self-diffusion falls monotonically with concentration (Table 4, Fig. 4): $D(Zn^{2+})$ 0.435 → 0.118, $D(Cl^-)$ 1.486 → 0.125, $D(H_2O)$ 2.01 → 0.62 (× 10^{-9} $m^2 \cdot s^{-1}$), as typically observed in molecular simulations of concentrated electrolytes [43, 44]. The Nernst–Einstein conductivity first rises with salt loading, reaches a broad maximum near 6 mol·kg^{-1} (σ_NE ≈ 30 S·m^{-1}; Fig. 5) and then declines at 10 mol·kg^{-1} ,which is the same rise-then-fall profile reported experimentally for aqueous $ZnCl_2$ [15] and for related zinc-salt electrolytes [45]. We emphasize that σ_NE is a relative, correlated-motion-neglecting estimator and benchmark its shape, not its absolute magnitude.

Table 4 Self-diffusion (10^{-9} $m^2 \cdot s^{-1}$) and Nernst–Einstein conductivity (mean ± standard error)

molality	D(Zn^{2+})	D(Cl^-)	D(H_2O)	σ_NE / ($S \cdot m^{-1}$)
1 $mol \cdot kg^{-1}$	0.435 ± 0.044	1.486 ± 0.120	2.01 ± 0.01	16.9
3 $mol \cdot kg^{-1}$	0.327 ± 0.056	0.798 ± 0.028	1.39 ± 0.09	28.4
6 $mol \cdot kg^{-1}$	0.279 ± 0.023	0.340 ± 0.013	1.09 ± 0.05	30.1
10 $mol \cdot kg^{-1}$	0.118 ± 0.006	0.125 ± 0.006	0.62 ± 0.03	17.1

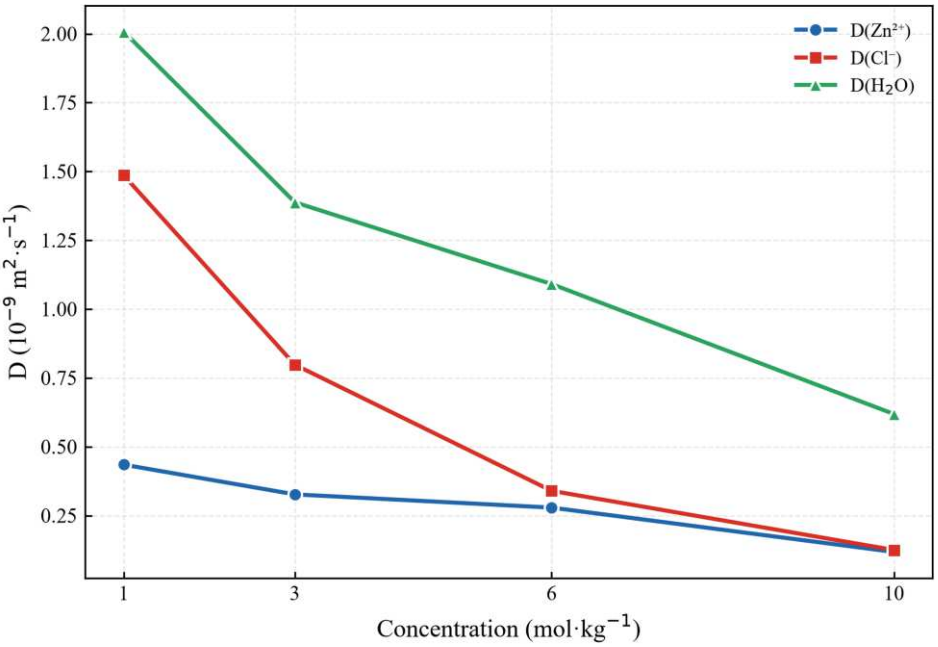


Fig. 4 Self-diffusion of Zn^{2+}, Cl^- and H_2O versus molality

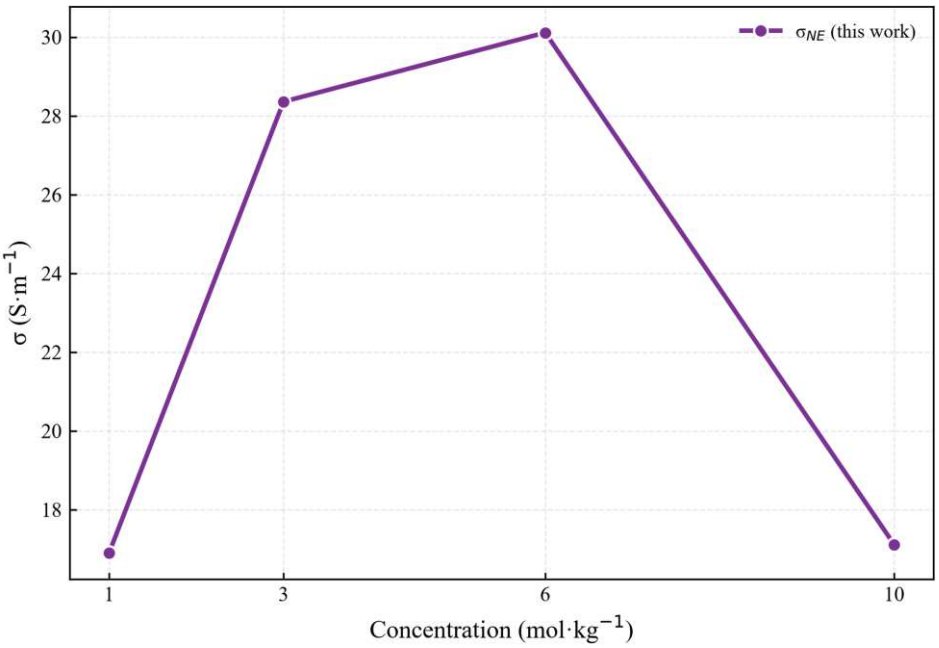


Fig. 5 Nernst–Einstein conductivity versus molality

3.5 ECC boundary test: the specific Zn–Cl term is essential

Fig. 6 and Table 5 compare the two ECC implementations at the 1 mol·kg^{-1} box. In the charge-only model (naive ECC, the version used in many classical studies), the CIP fraction is essentially unchanged at λ = 0.95 (41.3%) but collapses abruptly to 1.5% at λ = 0.90 and to zero by λ = 0.85: scaling charge alone, with no compensating specific term, erases Zn–Cl contact pairing. In the self-consistent model (scaled charge **plus** the dedicated Zn–Cl term), the CIP fraction stays at 33–50% across the whole λ = 1.00 → 0.75 window — the contact pair is retained even when the electrostatics are strongly reduced, because the specific Lennard-Jones term supplies the short, directional attraction that charge scaling removes [18, 26, 27] (Fig. 7). We caution that each λ point rests on a single 5 ns run with 12 Zn^{2+} ions (binomial standard error ≈ 10–14 percentage points), so the 33–50% variations within the self-consistent series are within statistical uncertainty; the qualitative contrast — complete collapse of the charge-only CIP versus its retention with the specific term — is nevertheless unambiguous.

This is the central methodological result: ECC repairs hydration electrostatics but cannot by itself reproduce Zn–Cl association; the dedicated specific Zn–Cl term is the ingredient that keeps contact ion pairing physical. It quantifies, on a classical model, the conclusion of Duboué-Dijon et al. [18] and the minimum physics required for quantitative $ZnCl_2$.

Table 5 ECC boundary test at 1 mol·kg^{-1}: CIP fraction versus charge-scaling λ for the two implementations

λ	CIP % (charge-only ECC)	CIP % (self-consistent ECC + σ_ZnCl)
1.00	44.0	50.0
0.95	41.3	50.0
0.90	1.5	33.3
0.85	0.0	41.7
0.75	≈ 0.0	41.7

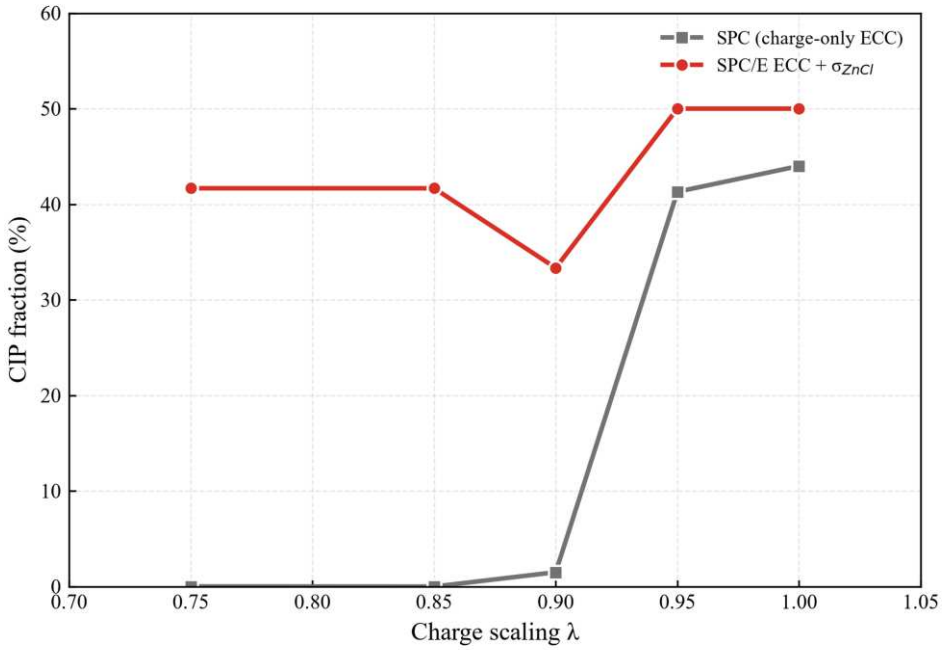


Fig. 6 ECC boundary test at 1 mol·kg^{-1}: CIP fraction versus charge-scaling λ for the charge-only ECC (grey) and the self-consistent ECC + specific Zn–Cl term (red)

3.6 Hydration-shell residence dynamics

To characterize how dynamically stable the Zn^{2+} first shell is and how it evolves with concentration, we computed the residence-time correlation function R(t) — the probability that a water (OW) or chloride (Cl^-) molecule that is in the first shell at t_0 stays there continuously until $t_0 + t$ (Fig. 7). R(t) decays only slowly. For first-shell water, R_OW(2 ns) is 0.79 at 1–3 mol·kg^{-1} and drops to 0.61–0.66 at 6–10 mol·kg^{-1} (Table 6), corresponding to nanosecond water residence times, which is far longer than the tens-of-picosecond values typical of weakly hydrated monovalent ions [46, 47], and consistent with hydration-residence analysis in other aqueous salt systems [48]. This is the expected signature of the strongly hydrated, octahedrally coordinated Zn^{2+} ion, and it highlights the contrast between Zn^{2+} and soft ions that the SPC/E-based model reproduces. Importantly, R_OW(2 ns) decreases from ≈ 0.79 (1–3 mol·kg^{-1}) to ≈ 0.61 (10 mol·kg^{-1}): as chloride displaces water (Sect. 3.2), the reduced first-shell water population exchanges faster , which is consistent with the water-network changes reported in highly concentrated electrolytes [49]. Chloride behaves oppositely: R_Cl(2 ns) stays ≥ 0.91 at all concentrations and is highest at 6–10 mol·kg^{-1} (0.94-0.95), showing that once a Cl^- binds to Zn^{2+} it tends to remain ,which is consistent with the growth of stable chloro-complexes at high loading. We also note that R_Cl(2 ns) ≈ 0.94 corresponds, under a simple exponential decay, to a chloride residence time of ~30 ns, i.e. only ≈ 1.5 residence intervals over the 50 ns runs; the species populations of Sect. 3.2 should therefore be read as semi-quantitative, although their concentration trends are robust.

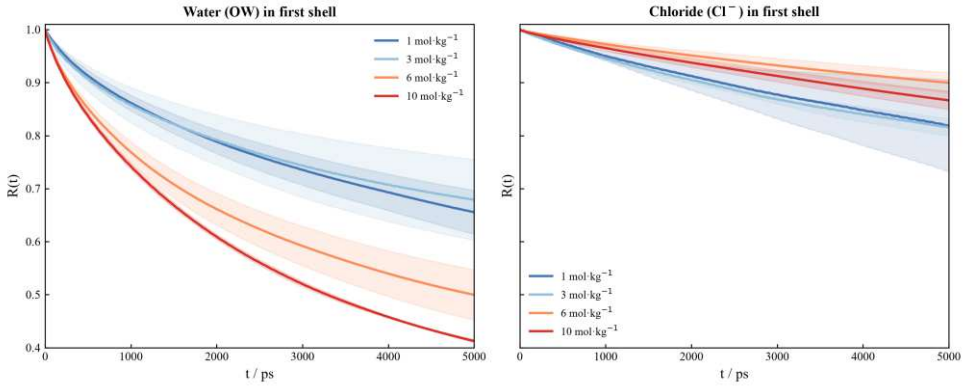


Fig. 7 Residence-time correlation functions R(t) for first-shell water (OW, left) and chloride (Cl^-, right), averaged over three replicas at each concentration

3.7 First-shell water geometry and orientation

Two further hydration-shell diagnostics, following the analysis applied to weakly hydrated monovalent ions [46], establish the orientational and geometric arrangement of the first-shell water. The distribution of the water dipole (DM) vector relative to the Zn–O axis peaks at cos θ ≈ 1 (Fig. 8): for 91% (1 mol·kg^{-1}) and 88% (3 mol·kg^{-1}) of first-shell water molecules the dipole makes an angle < 60° with the Zn–O vector, i.e. the oxygen points to Zn^{2+} and the hydrogens point outward. Consistently, the O–H bond vector peaks near cos θ ≈ 0.5–0.6 (≈ 52°), the value expected for this dipole-inward orientation — the orientational signature of a strongly hydrated (kosmotropic) ion [50, 51, 52]. The OW–Zn–OW angle distribution (Fig. 9) shows a strong peak near 90° with a secondary feature near 180°, signatures of an octahedral (six-coordinate) or trigonal-bipyramidal (five-coordinate) first shell, which is the same geometry reported for Zn^{2+} and Au^+ in aqueous solution [16, 46], and broadly consistent with the orientational ordering of water around ions in concentrated solutions [53, 54]. Table 6 summarizes the hydration-shell quantities.

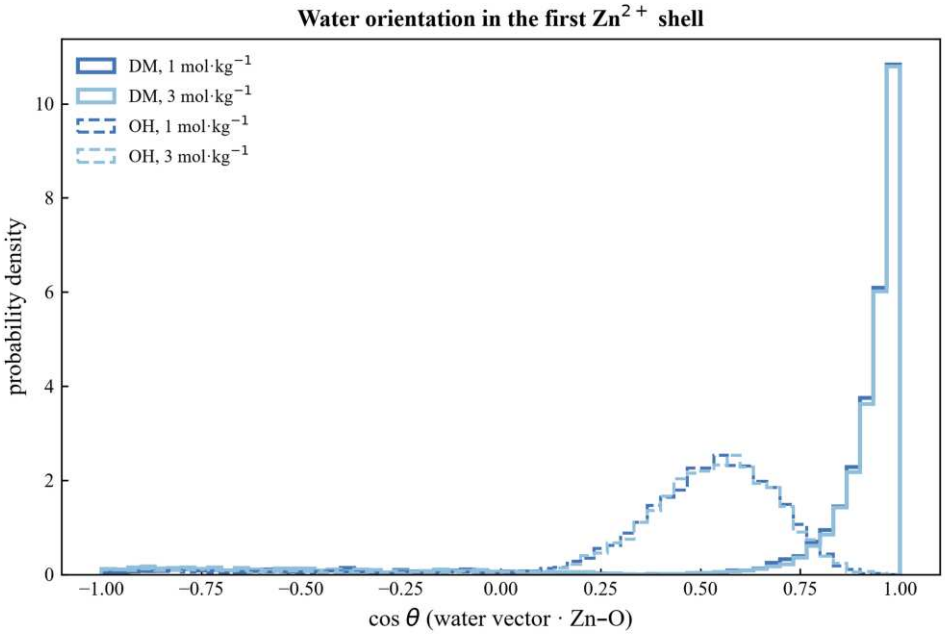


Fig. 8 Distributions of the water dipole (DM) and O–H vectors relative to the Zn–O axis in the first Zn^{2+} shell at 1 and 3 $mol \cdot kg^{-1}$

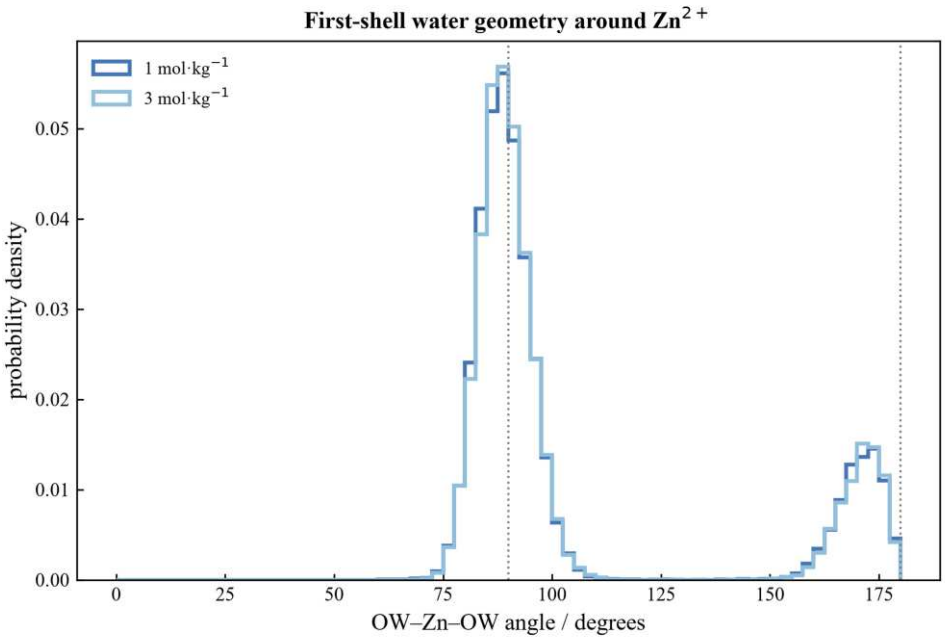


Fig. 9 OW–Zn–OW angle distribution in the first Zn^{2+} shell at 1 and 3 $mol \cdot kg^{-1}$ (vertical dashed lines mark 90° and 180°)

Table 6 Hydration-shell indicators at each concentration (R_OW, R_Cl = residence correlation at 2 ns; DM fraction = first-shell waters with dipole–Zn–O angle < 60°; orientation limited to 1–3 $mol \cdot kg^{-1}$)

molality	CN(Zn–O)	CN(Zn–Cl)	R_OW(2 ns)	R_Cl(2 ns)	DM < 60° fraction
1 $mol \cdot kg^{-1}$	5.47	0.50	0.79	0.91	0.91
3 $mol \cdot kg^{-1}$	4.67	0.94	0.79	0.91	0.88
6 $mol \cdot kg^{-1}$	3.09	1.93	0.66	0.95	—
10 $mol \cdot kg^{-1}$	2.63	2.20	0.61	0.94	—

4 Discussion and Limitations

On a uniform 1–10 mol·kg^{-1} series with a self-consistent, NDIS/ab initio-validated force field and sampling long enough for ligand exchange everywhere, we obtain a quantitative and physically consistent picture. The monotonic dehydration–chloride substitution (CN(Zn–O) 5.47 → 2.63, CN(Zn–Cl) 0.50 → 2.20; species $[Zn(H_2O)_6]^{2+}$ → $[ZnCl_3]^-$/$[ZnCl_4]^{2-}$) reproduces the species evolution reported for aqueous $ZnCl_2$ [15, 16, 37, 38, 40], and the first-shell distances align with the neutron-scattering/ab initio benchmarks [18]. The transport picture is likewise consistent with experiment: self-diffusion falls monotonically while the conductivity passes through a maximum near 6 mol·kg^{-1},which corroborates the rise-then-fall profile of concentrated $ZnCl_2$ [15] and of related zinc-salt electrolytes [45]. Table 7 cross-references the main observations of this work with the literature anchors.

The distinct contribution of this work is the ECC boundary test (Sect. 3.5). By holding every parameter fixed and toggling only the specific Zn–Cl term, we isolate the two failure modes of classical $ZnCl_2$ modelling and show they require different remedies:

- Full charges over-bind the contact pair (and over-estimate σ), because there is no polarization to screen the bare +2/−1 electrostatics.

- Charge-only ECC erases the contact pair, because reducing the charges removes the (already too weak) electrostatic attraction without adding the partly covalent short-range attraction that real Zn–Cl bonds have.

- Scaled charge + specific Zn–Cl term retains a physical contact pair while still improving hydration distances — the self-consistent path validated against experiment [18].

Table 7 Observation cross-reference (this work vs. literature)

Observation	This work	Literature anchor
Dehydration–chloride substitution	$[Zn(H_2O)_6]^{2+}$ → $[ZnCl_3]^-$/$[ZnCl_4]^{2-}$	[15] $[Zn(H_2O)_6]^{2+}$ → $[ZnCl_2(H_2O)_4]$; [37, 38] species progression; [16] high-Cl $ZnCl_x$ species
First-shell distances	Zn-O 0.209-0.212 nm; Zn-Cl 0.212-0.223 nm	[18] Zn-O ≈ 0.210 nm, Zn-Cl ≈ 0.225 nm; [16] Zn-Cl ≈ 0.229 nm
Contact pairing grows with concentration	CIP 50% → high plateau	[15] Zn-Cl CIP (0.228 nm) tied to conductivity fall
Conductivity	rise then fall, max near 6 mol·kg^{-1}	[15, 45] rise-then-fall of $ZnCl_2$ conductivity
ECC limit for Zn	charge-only ECC erases CIP (λ ≤ 0.90); +specific term retains it	[18] ECC repairs hydration but Zn needs a specific/covalent term

Limitations. (i) This remains a non-polarizable, point-charge model. Even the self-consistent set represents the partly covalent Zn–Cl bond only through a strengthened Lennard-Jones term; the contact-ion-pair fraction and the chloride-bridged multi-Zn (AGG) population are therefore expected to be over- and under-estimated respectively, and we report them as structural indicators rather than thermodynamically exact populations. Polarizable simulations of Zn^{2+} in water indicate that explicit polarization mainly refines hydration distances and free energies rather than the coordination picture [55]. (ii) The ε of the dedicated Zn–Cl term is not tabulated in the main text of [18]; we used the Lorentz–Berthelot geometric mean ($\sqrt{(1.046 \times 0.4928)} \approx 0.718$ kJ·mol^{-1}) rather than a fitted value, and the sensitivity of the results to this choice has not been systematically scanned — a worthwhile robustness check for future work, although the ECC boundary test of Sect. 3.5 holds the Zn–Cl Lennard-Jones parameters fixed and is therefore independent of ε. (iii) The Nernst–Einstein conductivity neglects correlated (Onsager) motion; we benchmark only the shape of σ versus concentration, not absolute values. (iv) The ECC λ scan was run at a single concentration (1 mol·kg^{-1}); the λ response may differ at higher concentration, where the specific term plays a larger role. (v) Experimental viscosity and Raman speciation are

cited qualitatively, not fitted. (vi) The simulation boxes are small — edge lengths of only a few nanometres, comparable to twice the 0.8 nm cutoff at 10 mol·kg^{-1} — so finite-size effects on the diffusion coefficients and on the extent of aggregation cannot be excluded, and no finite-size (Yeh–Hummer) correction was applied.

5 Conclusions

Using a self-consistent, neutron-scattering/ab initio-validated force field (SPC/E water + ECC-scaled Zn^{2+}/Cl^- + a dedicated Zn–Cl term) and sampling long enough for ligand exchange at every concentration, we obtained a quantitative description of aqueous $ZnCl_2$ across 1–10 mol·kg^{-1}: monotonic dehydration–chloride substitution, first-shell distances matching experiment, a rise-then-fall conductivity with a maximum near 6 mol·kg^{-1}, and a clear species progression toward higher chloro-complexes. The ECC boundary test demonstrates the key methodological point: effective charge scaling repairs hydration electrostatics but must be combined with a dedicated Zn–Cl interaction to retain ion association — quantifying the minimum physics a classical model needs for quantitative $ZnCl_2$, and framing the role of specific/covalent terms in non-polarizable descriptions.

Author Contributions Dan Ji: writing – original draft, visualization, software; Xiaolin Li: validation, writing – review & editing; Yue Yu: reference arrangement

Funding The authors affirm that this study did not receive any financial assistance for purposes of research, authorship, or publication.

Declarations Competing interests: the authors declare no competing interests. Data availability: the GROMACS input files, analysis scripts and the data underlying all figures and tables are available from the corresponding author on reasonable request.

References

1. Fang, G., Zhou, J., Pan, A., Liang, S.: Recent advances in aqueous zinc-ion batteries. ACS Energy Lett. 3, 2480–2501 (2018)
2. Niu, Z., Chen, J.: Energy storage chemistry in aqueous zinc metal batteries. ACS Energy Lett. 5, 3569–3590 (2020)
3. Dong, Y., Hu, H., Liang, P., Xue, L., Chai, X., Liu, F., Yu, M., Cheng, F.: Dissolution, solvation and diffusion in low-temperature zinc electrolyte design. Nat. Rev. Chem. 9, 102–117 (2025)
4. Suo, L., Borodin, O., Gao, T., Olguin, M., Ho, J., Fan, X., Luo, C., Wang, C., Xu, K.: Water-in-salt electrolyte enables high-voltage aqueous lithium-ion chemistries. Science 350, 938–943 (2015)
5. Zhang, C., Holoubek, J., Wu, X., Daniyar, A., Zhu, L., Chen, C., Leonard, D.P., Rodríguez-Pérez, I.A., Jiang, J.-X., Fang, C., Ji, X.: A $ZnCl_2$ water-in-salt electrolyte for a reversible Zn metal anode. Chem. Commun. 54, 14097–14099 (2018)
6. Rudolph, W.W., Pye, C.C.: Zinc(II) hydration in aqueous solution: a Raman spectroscopic investigation and an ab initio molecular orbital study of zinc(II) water clusters. J. Solution Chem. 28, 1045–1070 (1999)
7. Ohtaki, H., Radnai, T.: Structure and dynamics of hydrated ions. Chem. Rev. 93, 1157–1204 (1993)
8. Pillai, S.B., Wilcox, R.J., Hillis, B.G., Losey, B.P., Martin, J.D.: Understanding the water-in-salt to salt-in-water characteristics across the zinc chloride:water phase diagram. J. Phys. Chem. B 126, 2265–2278 (2022)
9. Ji, X.: A perspective of $ZnCl_2$ electrolytes: the physical and electrochemical properties. eScience 1, 99–107 (2021)
10. Qiu, M., Sun, P., Han, K., Pang, Z., Du, J., Li, J., Chen, J., Wang, Z.L., Mai, W.: Tailoring water structure with high-tetrahedral-entropy for antifreezing electrolytes and energy storage at −80 °C. Nat. Commun. 14, 601 (2023)
11. Zhang, Q., Ma, Y., Lu, Y., Li, L., Wan, F., Zhang, K., Chen, J.: Modulating electrolyte structure for ultralow temperature aqueous zinc batteries. Nat. Commun. 11, 4463 (2020)
12. Rampal, N., Wang, H.-W., Biriukov, D., Brady, A.B., Neuefeind, J.C., Předota, M., Stack, A.G.: Local molecular environment drives speciation and reactivity of ion complexes in concentrated salt solution. J. Mol. Liq. 340, 116898 (2021)
13. Brahma, D., Avula, N.V.S., Balasubramanian, S.: Hydration environment of complexes and their dynamics in aqueous zinc chloride solutions. J. Phys. Chem. B 130, 6412–6421 (2026)
14. Panagiotopoulos, A.Z., Yue, S.: Dynamics of aqueous electrolyte solutions: challenges for simulations. J. Phys. Chem. B 127, 430–437 (2023)

15. Xu, Z., Zhang, Y., Guo, X., Li, F., Liu, J., Fei, L., Zhao, Y., Wang, S., Wang, J., Bi, J., Zhang, P., Yuan, J., Ji, Z.: Study on the correlation between the microstructure and physical properties of $ZnCl_2$ aqueous solution. J. Phys. Chem. B 129, 2259–2270 (2025)

16. Harris, D.J., Brodholt, J.P., Harding, J.H., Sherman, D.M.: Molecular dynamics simulation of aqueous $ZnCl_2$ solutions. Mol. Phys. 99, 825–833 (2001)

17. Li, Y.-Y., Wang, M., Wang, C.-C., Zhang, Q.-W., Yi, H.-B.: Distinctive hydration dynamics around highly coordinated Cu^{2+}/Zn^{2+}-chloride complexes: a molecular dynamics simulation study. J. Mol. Liq. 314, 113619 (2020)

18. Duboué-Dijon, E., Mason, P.E., Fischer, H.E., Jungwirth, P.: Hydration and ion pairing in aqueous Mg^{2+} and Zn^{2+} solutions: force-field description aided by neutron scattering experiments and ab initio molecular dynamics simulations. J. Phys. Chem. B 122, 3296–3306 (2018)

19. Cao, C., Kingan, A., Hill, R.C., Kuang, J., Wang, L., Zhang, C., Carbone, M.R., van Dam, H., Yoo, S., Yan, S., Takeuchi, E.S., Takeuchi, K.J., Wu, X., Abeykoon, A.M.M., Marschilok, A.C., Lu, D.: Resolving the solvation structure and transport properties of aqueous zinc electrolytes from salt-in-water to water-in-salt using neural network potential. PRX Energy 4, 023004 (2025)

20. Tkachenko, A.V., Cao, C., Marschilok, A.C., Lu, D.: Dehydration-driven ion aggregation and the onset of gelation in $ZnCl_2$ solution. PRX Energy 5, 033012 (2026)

21. Omranpour, A., De Hijes, P.M., Behler, J., Dellago, C.: Perspective: atomistic simulations of water and aqueous systems with machine learning potentials. J. Chem. Phys. 160, 170901 (2024)

22. Friederich, P., Häse, F., Proppe, J., Aspuru-Guzik, A.: Machine-learned potentials for next-generation matter simulations. Nat. Mater. 20, 750–761 (2021)

23. Abraham, M.J., Murtola, T., Schulz, R., Páll, S., Smith, J.C., Hess, B., Lindahl, E.: GROMACS: high performance molecular simulations through multi-level parallelism from laptops to supercomputers. SoftwareX 1, 19–25 (2015)

24. Hess, B., Kutzner, C., van der Spoel, D., Lindahl, E.: GROMACS 4: algorithms for highly efficient, load-balanced, and scalable molecular simulation. J. Chem. Theory Comput. 4, 435–447 (2008)

25. Berendsen, H.J.C., Grigera, J.R., Straatsma, T.P.: The missing term in effective pair potentials. J. Phys. Chem. 91, 6269–6271 (1987)

26. Leontyev, I.V., Stuchebrukhov, A.A.: Electronic continuum model for molecular dynamics simulations of biological molecules. J. Chem. Theory Comput. 6, 1498–1508 (2010)

27. Leontyev, I.V., Stuchebrukhov, A.A.: Accounting for electronic polarization in non-polarizable force fields. Phys. Chem. Chem. Phys. 13, 2613–2626 (2011)

28. Joung, I.S., Cheatham, T.E., III.: Determination of alkali and halide monovalent ion parameters for use in explicitly solvated biomolecular simulations. J. Phys. Chem. B 112, 9020–9041 (2008)

29. Bussi, G., Donadio, D., Parrinello, M.: Canonical sampling through velocity rescaling. J. Chem. Phys. 126, 014101 (2007)

30. Parrinello, M., Rahman, A.: Polymorphic transitions in single crystals: a new molecular dynamics method. J. Appl. Phys. 52, 7182–7190 (1981)

31. Essmann, U., Perera, L., Berkowitz, M.L., Darden, T., Lee, H., Pedersen, L.G.: A smooth particle mesh Ewald method. J. Chem. Phys. 103, 8577–8593 (1995)

32. Allen, M.P., Tildesley, D.J.: Computer Simulation of Liquids, 2nd edn. Oxford University Press, Oxford (2017)

33. Frenkel, D., Smit, B.: Understanding Molecular Simulation: From Algorithms to Applications, 3rd edn. Academic Press, London (2023)

34. Cauët, E., Bogatko, S., Weare, J.H., Fulton, J.L., Schenter, G.K., Bylaska, E.J.: Structure and dynamics of the hydration shells of the Zn^{2+} ion from ab initio molecular dynamics and combined ab initio and classical molecular dynamics simulations. J. Chem. Phys. 132, 194502 (2010)

35. D'Angelo, P., Zitolo, A., Ceccacci, F., Caminiti, R., Aquilanti, G.: Structural characterization of zinc(II) chloride in aqueous solution and in the protic ionic liquid ethyl ammonium nitrate by x-ray absorption spectroscopy. J. Chem. Phys. 135, 154509 (2011)

36. Guardia, E., Sesé, G., Padró, J.A., Kalko, S.G.: Molecular dynamics simulation of Mg^{2+} and Ca^{2+} ions in water. J. Solution Chem. 28, 1113–1126 (1999)

37. Irish, D.E., McCarroll, B., Young, T.F.: Raman study of zinc chloride solutions. J. Chem. Phys. 39, 3436–3444 (1963)

38. Dhakal, D., Driscoll, D.M., Govind, N., Stack, A.G., Rampal, N., Schenter, G.K., Mundy, C.J., Fister, T.T., Fulton, J.L., Balasubramanian, S., Seidler, G.T.: The evolution of solvation symmetry and composition in Zn halide aqueous solutions from salt-in-water to water-in-salt. Phys. Chem. Chem. Phys. 25, 22650–22661 (2023)

39. Kruh, R.F., Standley, C.L.: An X-ray diffraction study of aqueous zinc chloride solutions. Inorg. Chem. 1, 941–943 (1962)

40. Sethi, A., Rajeev, C., Kumar, A.U., Sharma, P., Sunda, A.P., Dhavale, V.M.: Assessing the impact of antisolvent-regulated $ZnCl_2$ water-in-salt electrolyte on solvation structure: a multiscale computational validation for aqueous Zn-ion battery application. J. Mater. Chem. A 12, 23049–23058 (2024)

41. Mei, Y., Sherman, D.M., Liu, W., Brugger, J., Etschmann, B., Testemale, D., Hazemann, J.-L.: Zinc complexation in chloride-rich hydrothermal fluids (25–600 °C): a thermodynamic model derived from ab initio molecular dynamics. Geochim. Cosmochim. Acta 150, 265–284 (2015)

42. Harris, D.J., Brodholt, J.P., Sherman, D.M.: Zinc complexation in hydrothermal chloride brines: results from ab initio molecular dynamics calculations. J. Phys. Chem. A 107, 1050–1054 (2003)

43. Ravikumar, B., Mynam, M., Rai, B.: Effect of salt concentration on properties of lithium ion battery electrolytes: a molecular dynamics study. J. Phys. Chem. C 122, 8173–8181 (2018)

44. Chliyah, S., Rabii, S., Lahmidi, A., Chtita, S., El Kouali, M., Errougui, A.: Molecular dynamics simulations of the solvation, dynamics, and dielectric properties of the energy storage system {$NaBF_4$–dimethyl sulfoxide} at different temperatures. J. Solution Chem. 55, 1142–1159 (2026)

45. Zhang, Y., Carino, E., Hahn, N.T., Becknell, N., Mars, J., Han, K.S., Mueller, K.T., Toney, M., Maginn, E.J., Tepavcevic, S.: Understanding the surprising ionic conductivity maximum in $Zn(TFSI)_2$ water/acetonitrile mixture electrolytes. J. Phys. Chem. Lett. 14, 11393–11399 (2023)

46. Saha, S., Bhadyopadhyay, D., Choudhury, N.: Solvation structure and dynamics of aqueous solutions of Au^+ ions: a molecular dynamics simulation study. J. Solution Chem. 52, 326–342 (2023)

47. Salmon, P.S., Bellissent-Funel, M.-C., Herdman, G.J.: The dynamics of aqueous Zn^{2+} solutions: a study using incoherent quasi-elastic neutron scattering. J. Phys.: Condens. Matter 2, 4297–4309 (1990)

48. Errougui, A., Lahmidi, A., Chtita, S., El Kouali, M., Talbi, M.: Hydration structures and dynamics of the sodium fluoride aqueous solutions at various temperatures: molecular dynamics simulations. J. Solution Chem. 52, 176–186 (2023)

49. Zhang, C., Yue, S., Panagiotopoulos, A.Z., Klein, M.L., Wu, X.: Dissolving salt is not equivalent to applying a pressure on water. Nat. Commun. 13, 822 (2022)

50. Laage, D., Hynes, J.T.: Reorientional dynamics of water molecules in anionic hydration shells. Proc. Natl. Acad. Sci. U.S.A. 104, 11167–11172 (2007)

51. Marcus, Y.: Effect of ions on the structure of water: structure making and breaking. Chem. Rev. 109, 1346–1370 (2009)

52. Laage, D., Stirnemann, G.: Effect of ions on water dynamics in dilute and concentrated aqueous salt solutions. J. Phys. Chem. B 123, 3312–3324 (2019)

53. Shi, R., Cooper, A.J., Tanaka, H.: Impact of hierarchical water dipole orderings on the dynamics of aqueous salt solutions. Nat. Commun. 14, 4616 (2023)

54. Agnew, H., Savoj, R., Rashmi, R., Savala, B., Paesani, F.: Molecular insights into the influence of ions on the water structure. II. Halide ions in solution. J. Phys. Chem. B 129, 6584–6593 (2025)

55. Wu, J.C., Piquemal, J.-P., Chaudret, R., Reinhardt, P., Ren, P.: Polarizable molecular dynamics simulation of Zn(II) in water using the AMOEBA force field. J. Chem. Theory Comput. 6, 2059–2070 (2010)